11th World Congress on Computational Mechanics (WCCM XI)
5th European Conference on Computational Mechanics (ECCM V)
6th European Conference on Computational Fluid Dynamics (ECFD VI)
E. Oñate, J. Oliver and A. Huerta (Eds)

A MULTI-SCALE MODEL OF MULTI-FLUID FLOWS TRANSPORT IN DUAL SATURATED-UNSATURATED HETEROGENEOUS POROUS MEDIA

William C. Radunz[1,2], Francisco B.S. Oliveira[3] and Jefferson L.M.A. Gomes[2]

[1] Department of Mechanical Engineering
School of Engineering, Federal University of Rio Grande do Sul (UFRGS)
Porto Alegre, Rio Grande do Sul, 90050-170, Brazil
e-mail: williamradunz@gmail.com - Web page: http://www.mecanica.ufrgs.br

[2] Environmental and Industrial Fluid Mechanics Group
School of Engineering, University of Aberdeen
Aberdeen, AB24 3UE, UK
e-mail: jefferson.gomes@abdn.ac.uk - Web page: http://www.abdn.ac.uk

[3] Department of Exact and Technological Sciences
State University of Santa Cruz (UESC)
Ilheus, Bahia, 45662-900, Brazil
e-mail: fbrunoso@gmail.com - Web page: http://www.uesc.br

Key words: Porous media, Finite element methods, Control volume, Discontinuous Galerkin, Multi-fluid flows, Multi-physics methods.

Abstract. This paper introduces a conservative computational multi-fluid porous media flows model able to exploit the latest mesh adaptivity methods on fully-unstructured tetrahedral grids. The model is based upon two key numerical characteristics: (a) novel family of P_nDG-P_{n+1} finite element pairs [1] and (b) a consistent overlapping control volume finite element method (CVFEM) formulation. In particular, the P_1DG-P_2 element (i.e., discontinuous and piecewise linear representation for velocity whilst continuous and piecewise quadratic shape functions are used to represent the pressure field) is introduced as the basis of the discretisation and also as the CVFEM counterpart. The formulation is applied to an unsaturated/saturated porous media system.

1 INTRODUCTION

Current generation of fluid flow models for porous media flows are very sophisticated, however they are often based on outdated computational methods (e.g. structured or block structured hexahedral FEM- and FDM-based discretisation). Since these methods are often at the heart of transport in porous media, it is vital that these methods are

updated in light of recent advances in computational methods and able to exploit the current state-of-the-art mesh-adaptive methods. The latter moves the mesh to follow flow features or interface, and adapts the structure of the mesh to produce optimal anisotropic resolution [11]. The computational effort is thus placed exactly where it is needed.

It is rather important to apply these new concepts in terms of research, as well as in industry. In oil exploration, typical recovery factors after primary and secondary oil recovery operations are between 35% and 45% [14] – this means that at least half of the oil content can not be effectively recovered. One way of optimising these operations is by improving our understanding of geophysical properties of hydrocarbon's reservoirs, but also developing more accurate models that help predicting multi-fluid flow in heterogeneous reservoirs.

In soil contamination problems, health risks associated with direct contact with the contaminant and/or its vapours have been investigated. In addition, these contaminants might affect groundwater aquifers and other sources of water supplies. This problem can be mitigated by excavating, containing and aerating the contaminated cross-section of soil, within other methods [15]. One way of improving environmental remediation is by using field measurements along with numerical simulation, hence the need for more sophisticated and reliable computational approaches [7]. Many phenomena arise from multi-fluid flow in porous media, one of which is known as viscous fingering, i.e., onset and propagation of instabilities in porous media flow caused by differences in viscosity, density and porous media morphological properties. Viscous fingering allows a wide spectrum of length scales to occur in the flow, which is rather important for applications in secondary and tertiary oil recovery [8]. It is widely reckoned that an approximated solution to the Richards equation in regions with steep gradients in saturation, as in wetting fronts, might yield inaccurate results [13]. Therefore, developing and optimising mesh-adaptivity algorithms are essential steps towards better prediction of multiphase porous media flow in all associated length-scales.

The main objective of this manuscript is to report the latest development of a generic FEM-based unstructured and adaptive-mesh multi-fluid model that can be applied to both inertia-dominated and porous media flows. In the simulations performed in this paper we used P_1DG-P_2 elements and the overlapping CVFEM model [6, 9] where scalar fields (e.g., volume fraction, concentration, density, etc) are represented in the control volume (CV) space and the velocity-pressure dual fields are embedded in FEM space with simultaneous projection into the CV space. High-order accurate downwind schemes on element boundaries on discontinuous scalar fields are flux-limited (based on NVD approach) to obtain bounded and compressive (capturing the interfaces) solutions. Section 2 summarises the numerical formulation used in this work, followed by description of the computational experiment. Finally, conclusions are drawn in Section 4.

2 NUMERICAL FORMULATION

2.1 Introduction

This section summarises the novel formulation to solve multiphase porous media flows - the overlapping control volume – discontinuous Galerkin finite element method (OCV-DGFEM). The method is based on twofold, an overlapping scheme for CV-FEM mixing formulation and the recently developed P_nDG-P_{n+1} family of finite element (FE) types. The underlying mass balance equations (eg, saturation, density, mass fraction, etc.) are solved in control volume space whereas a Petrov-Galerkin FEM is used to obtain the high order fluxes on the control volume boundaries which are limited to achieve bounded mass-based fields (e.g., positiveness of densities and saturations ranging from zero to one).

The family of P_nDG-P_{n+1} element pair was originally introduced by [2] (see also [3]) for geophysical fluid dynamics (GFD) applications. In particular, the P_1DG-P_2 element pair - linear discontinuous polynomial FE basis function for velocity (P_1DG) and quadratic polynomial FE basis function for pressure (P_2), was developed to represent the balance of geostrophic pressure and velocity without introducing spurious pressure modes. Any numerical discretisation that is not based upon quads and hexs meshes very often results in spurious pressure modes due to the unbalancing number of velocity and pressure degrees-of-freedom [1, 12]. However, tests on the P1DG-P2 element pair proved that this element is LBB stable and does not present spurious pressure modes on arbitrary unstructured meshes. Additionally, this family of FE when used with the OCV-DGFEM presented here results in the exact balance represented by the extended Darcy equation.

2.2 Overlapping CVFEM Formulation

Darcy's law for single phase flow can be extended for immiscible multiphase flow as

$$\mathbf{q}_k = -\frac{\mathcal{K}_{r_k}(S_k)\,\mathbf{K}}{\mu_k}\left(\nabla p_k - \mathbf{s}_{uk}\right), \tag{1}$$

where $\mathbf{q}_k$ is the $k\,(\in \{1, N_p\})$-phase Darcy flow rate. S, $\mathbf{K}$, $\mathcal{K}_{rk}(S_k)$, μ_k and ϕ are saturation, absolute permeability tensor, phase relative permeability, phase viscosity and porosity, respectively. s_u is a source term (eg., gravity force) associated with the force balance and p is the pressure. Defining the advective velocity averaged over the entire domain – $\mathbf{u}_k = \mathbf{q}_k/S_k$, then we may rewrite Eqn. 1,

$$\underline{\underline{\sigma}}_k \mathbf{u}_k = -\nabla p + \mathbf{s}_{uk}, \tag{2}$$

$\underline{\underline{\sigma}}_k$ can be treated as a numerical absorption term with coupled FE and control volume (CV) representation of the nonlinear convolution of saturation, relative permeabilities, porosity and permeability tensor fields. $\underline{\underline{\sigma}}_k$ is piecewise constant within each FE and is obtained via basis functions local to each CV within each element. Although this approach can be attractive due to high-order accuracy, the associate computational costs would be

prohibitive for simulations in complex 3D geometries and larger number of calculated fields. In order to overcome such major computational cost, overlapping (or hybrid) basis functions are introduced (see [6, 9]) to combine finite element representation for velocity and pressure and control volume representation for the saturation. The FE velocity and pressure basis function Q and P are defined as

$$u_k = \sum_{j=1}^{\mathcal{N}_u} Q_j u_{k,j} \quad \text{and} \quad p = \sum_{j=1}^{\mathcal{N}_p} P_j p_j \tag{3}$$

where $\mathcal{N}_p$ and $\mathcal{N}_u$ are the number of degrees of freedom for the FE velocity and pressure representations, respectively. The FEM solution, Ψ_{FEM}, is related to the CV solution, Ψ, by [5]

$$\int_\Omega N_i \left(\Psi_{\text{FEM}} - \Psi\right) dV = 0, \quad \forall i \in \{1, 2, ..., \mathcal{N}\},$$

where N_i is the FE basis function associated with the i-th degree of freedom. In addition, the FEM representation of Ψ can be expressed as,

$$\Psi_{\text{FEM}} = \sum_{j=1}^{\mathcal{N}} N_j \Psi_{\text{FEM}j}.$$

For the control volume space, the basis function M_j is used and correlated to N_i by,

$$\mathbf{B}\underline{\mathbf{\Psi}}_{\text{FEM}} = \mathbf{Q}\underline{\mathbf{\Psi}}, \tag{4}$$

with

$$\mathbf{B} = \int_\Omega N_i N_j \, dV \quad \text{and} \quad \mathbf{Q} = \int_\Omega N_i M_j \, dV,$$

and

$$\underline{\mathbf{\Psi}}_{\text{FEM}} = \left(\Psi_{\text{FEM}1}, \ldots, \Psi_{\text{FEM}\mathcal{N}}\right)^T \text{ and } \underline{\mathbf{\Psi}} = \left(\Psi_1, \Psi_2, \ldots, \Psi_{\mathcal{M}}\right)^T$$

Each component of the weak form of Eqn. 2 is tested with the velocity basis function space to obtain:

$$\sum_E \int_{\Omega_E} Q_i \left(\underline{\underline{\sigma}}_k \mathbf{u}_k + \nabla p - \mathbf{s}_{u_k}\right) dV + \frac{1}{2} \oint_{\Gamma_E} Q_i \mathbf{n} \left(p - p_{nab}\right) d\Gamma + \oint_{\Gamma_\Omega} Q_i \mathbf{n} \left(p - p_{bc}\right) d\Gamma = \mathbf{0}, \tag{5}$$

where Ω_E and Γ_E are the volume and boundary of element E, respectively, and Γ_Ω is the boundary of the computational domain. The pressure appearing in the jump condition p_{nab} is the pressure value on the other side of the element boundary neighbouring element E. Equation 5 can be represented, in matrix form, as:

$$\mathbf{M}_\sigma \underline{\mathbf{u}} = -\mathbf{C}\underline{\mathbf{p}} + \underline{\mathbf{s}}_u, \tag{6}$$

where $\mathbf{M}_\sigma$, $\mathbf{C}$ and $\mathbf{s}_u$ are the sigma-weighted mass matrix, gradient matrix and discretised source terms, respectively [9].

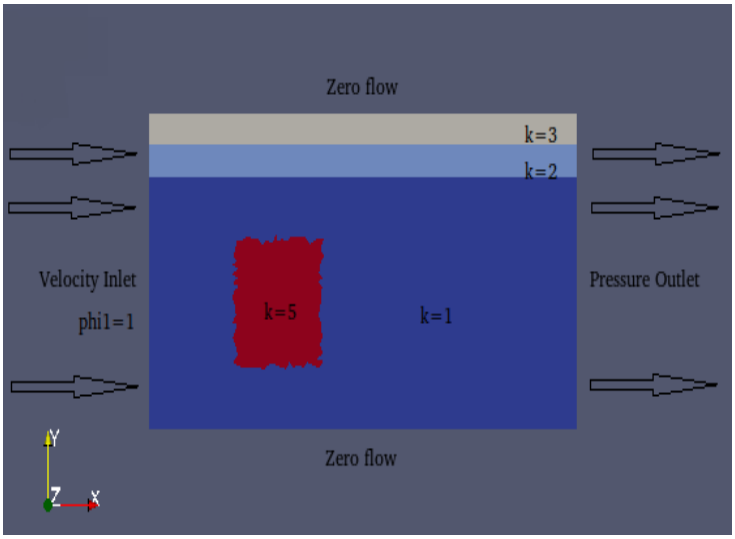

Figure 1: Schematics of the simulated domain with $\mathcal{K}_i$.

2.3 Saturation and Global Mass Conservation Equations

The saturation equation,

$$\phi \frac{\partial S_k}{\partial t} + \nabla \cdot (\mathbf{u}_k S_k) = s_{cty,k}, \tag{7}$$

can be discretised in space by testing with CV basis functions M_i with the θ-method [5] in time. Summing the discretised equation over all N_k phases, the global continuity equation is obtained,

$$\sum_{k=1}^{N_k} \left\{ \int_\Omega M_i \frac{\phi \left({S_{ki}}^{n+1} - {S_{ki}}^{n} \right)}{\Delta t} dV + \oint_{\Gamma_{CV\,i}} \left[\theta^{n+\frac{1}{2}} \mathbf{n} \cdot \mathbf{u}_k^{n+1} S_k^{n+1} + \left(1 - \theta^{n+\frac{1}{2}} \right) \mathbf{n} \cdot \mathbf{u}_k^n S_k^n \right] d\Gamma - \int_\Omega M_i s_{cty,k}^{n+\theta} \, dV \right\} = 0, \tag{8}$$

with the mass conservation constraint,

$$\sum_{k=1}^{\mathcal{N}_k} {S_{ki}}^{n} = 1, \quad \forall n,$$

in matrix form Eqn. 8 becomes,

$$\mathbf{B}^T \underline{\mathbf{u}}^{n+1} = \underline{\mathbf{s}}_p. \tag{9}$$

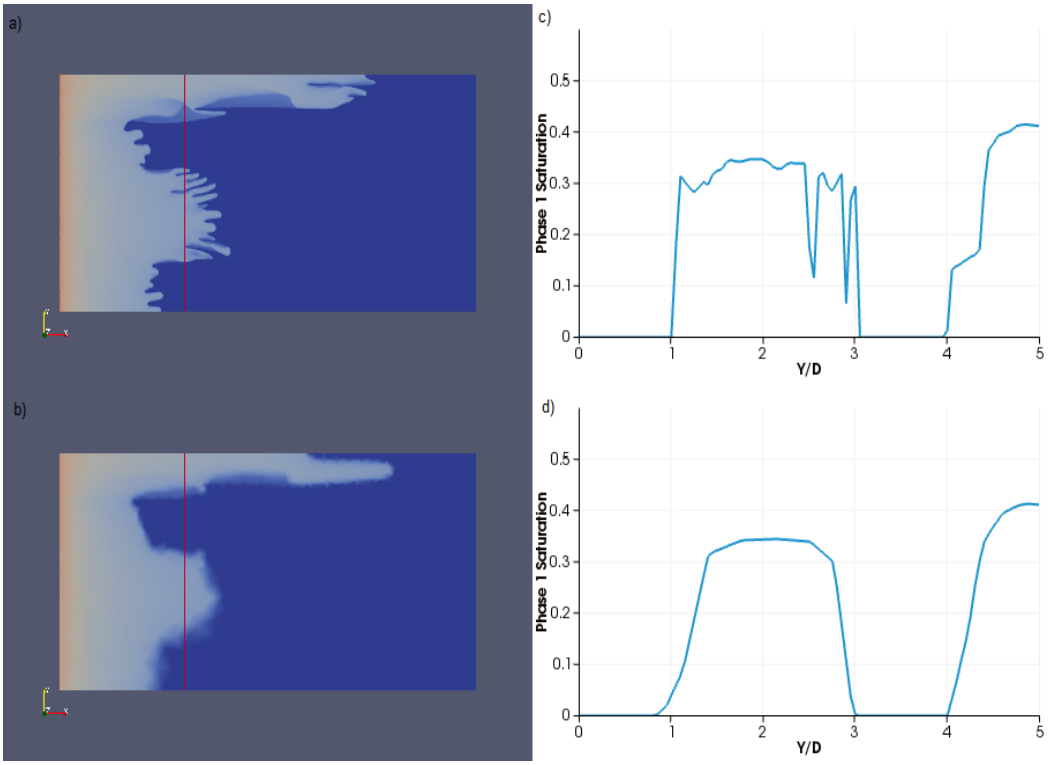

Figure 2: Snapshots (at $t = 0.68$ s) for the simulation performed with adaptive (top left) and fixed mesh grids. Saturation profile (along the indicated vertical line) is shown in r.h.s. for both simulations.

2.4 Solving the Linear Equations

The global mass balance equation (Eqn. 9) and force balance equations (Eqn. 6) are solved by vanishing the velocity term and solving the system of equations for pressure. At time level $n+1$, Eqns. 6 and 9 can be rewritten as:

$$\begin{cases} \mathbf{M}_\sigma \underline{\mathbf{u}}^{n+1} &= \mathbf{C}\underline{\mathbf{p}}^{n+1} + \underline{\mathbf{s}}_u^{n+1} \\ \mathbf{B}^T \underline{\mathbf{u}}^{n+1} &= \underline{\mathbf{s}}_p^{n+1} \end{cases}$$

Application of a discontinuous FEM for velocity leads to a block-diagonal $\mathbf{M}_\sigma$ matrix that can be readily inverted, each block being local to an element. This system of equation can be rewritten to produce the pressure equation,

$$\mathbf{B}^T\mathbf{M}_\sigma^{-1}\mathbf{C}\underline{\mathbf{p}}^{n+1} = \underline{\mathbf{s}}_p^{n+1} - \mathbf{B}^T\mathbf{M}_\sigma^{-1}\underline{\mathbf{s}}_u^{n+1}. \tag{10}$$

The computationally demanding effort to solve the pressure matrix equation (arising from the fully discontinuous FEM formulation) is achieved using a multigrid-like approach (see [6] for further details).

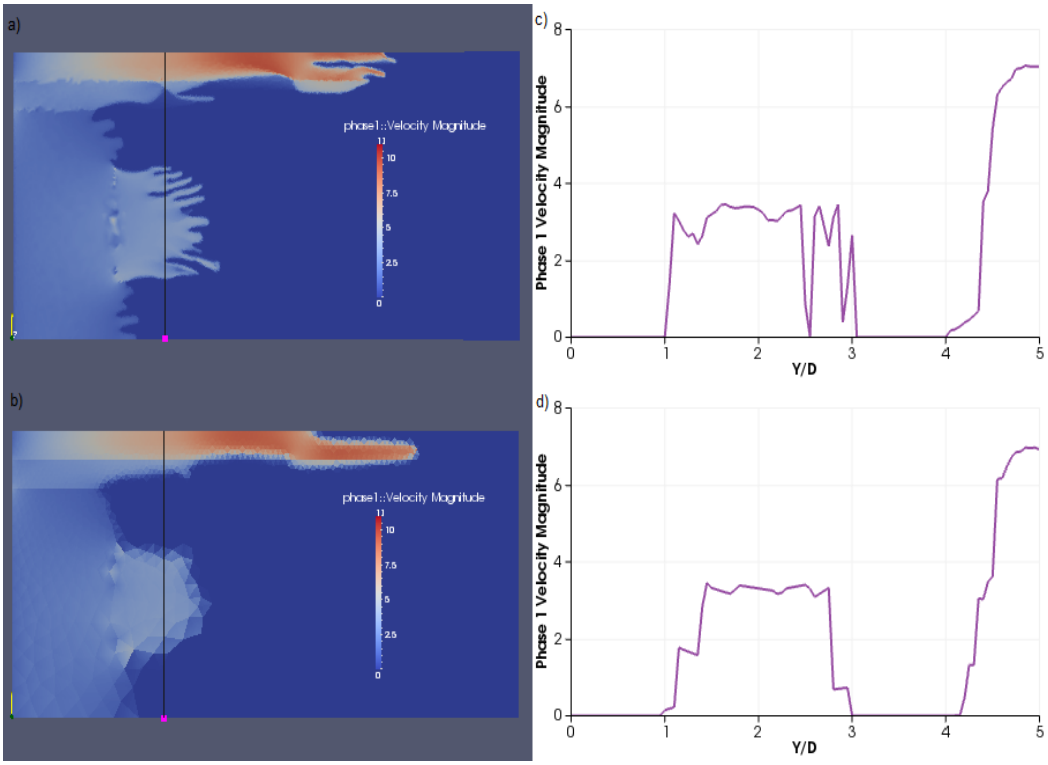

Figure 3: Snapshots (at $t = 0.68$ s) for the simulation performed with adaptive (top left) and fixed mesh grids. Velocity profile (along the indicated vertical line) is shown in r.h.s. for both simulations.

3 RESULTS

Here we simulated a non-linear advection (Richard) equation for the relative saturation fluid phases representing two-phase immiscible flows in porous media. The fluid 1 is injected at a velocity $u_1\phi = 1$. On the outlet boundary, the pressure level is set to zero and all remaining boundary conditions are naturally applied. Fixed time-step sizes of 5×10^{-4} and 2×10^{-4} were used in the coarse and adaptive mesh grids, respectively (see [10, 11] for more details on tetrahedral mesh adaptivity for FEM calculations). All simulations shown in this Section used the overlapping mixed FEM (Section 2.2) with a piecewise linear variation of the velocity within each element and quadratic pressure (P_1DG-P_2). Saturation is colocated at the pressure nodes and although it is calculated using a CV formulation, a FEM interpolation is used to form the high-order fluxes. The 2-D domain heterogeneity is introduced by imposing 4 distinct absolute permeabilities ($\mathbf{K}$) as shown in Fig. 1. There is no flow across the bottom and top edges and the initial velocity of Fluid 2 is set to zero. In the current set of numerical simulations, mobility ratio is set to 10 and gravity is assumed negligible.

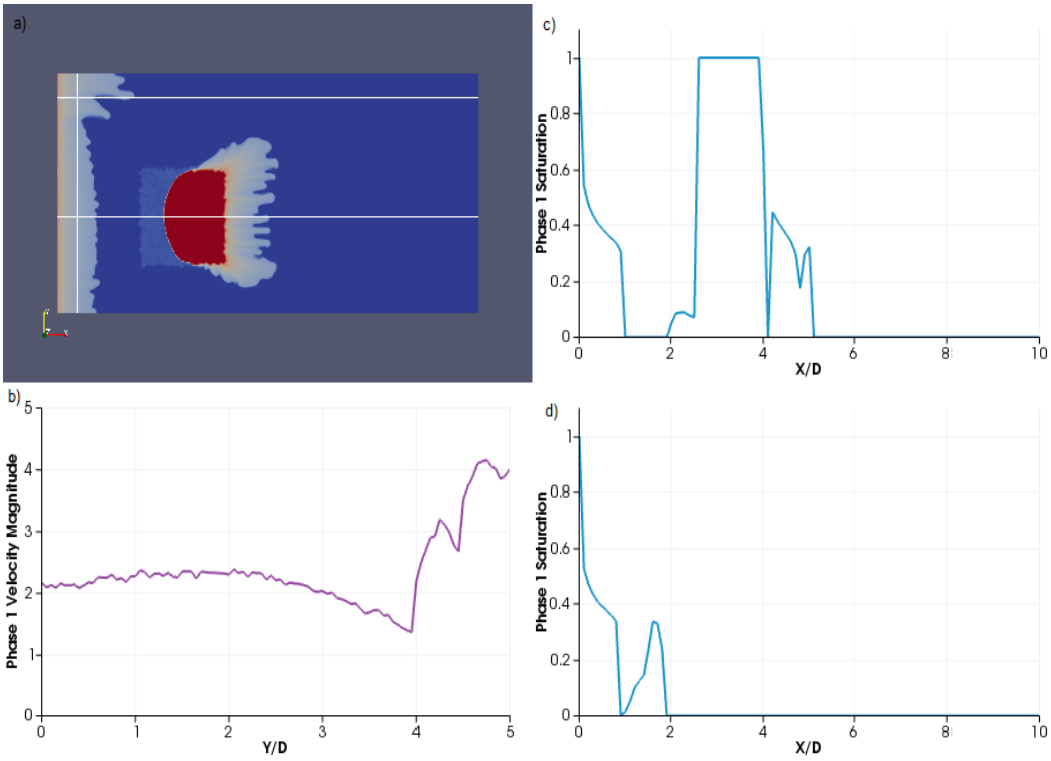

Figure 4: Snapshot (at $t = 0.19$ s) for the simulation performed with heterogeneous media, dual saturated/unsaturated fields (top left) and adaptive mesh. Saturation and velocity profiles (along the indicated vertical lines) are shown.

3.1 Case 1: Heterogeneous Porous Media Fully Saturated with Fluid 2

In this set of simulations, saturation of phase 2 is set to one throughout the whole domain ($S_2 = 1$) whereas pure Fluid 1 is injected from the left boundary. Figures 2 and 3 shows simulations performed with fixed coarse (bottom left: 2415 nodes in 4828 triangular elements – top left of Fig. 5) and adaptive (top left: max 10700 nodes in 20500 elements) mesh grids. The adaptive mesh, focusing the resolution in the saturation fronts, leads to the explicit formation of fingers resulted from instability in the pressure field fostered by a high mobility ratio. It can also be seen two regions with intermediate permeability (top of the domain, $\mathbf{K}_1 = 2$ and $\mathbf{K}_2 = 3$, and the central high-permeability square-region (with $\mathbf{K}_3 = 5$), in which the flow accelerates. The high-permeability square-region, where most of the fingers are formed, are more pronounced in the simulation performed with fine (and adaptive) mesh, as shown in Fig. 3.

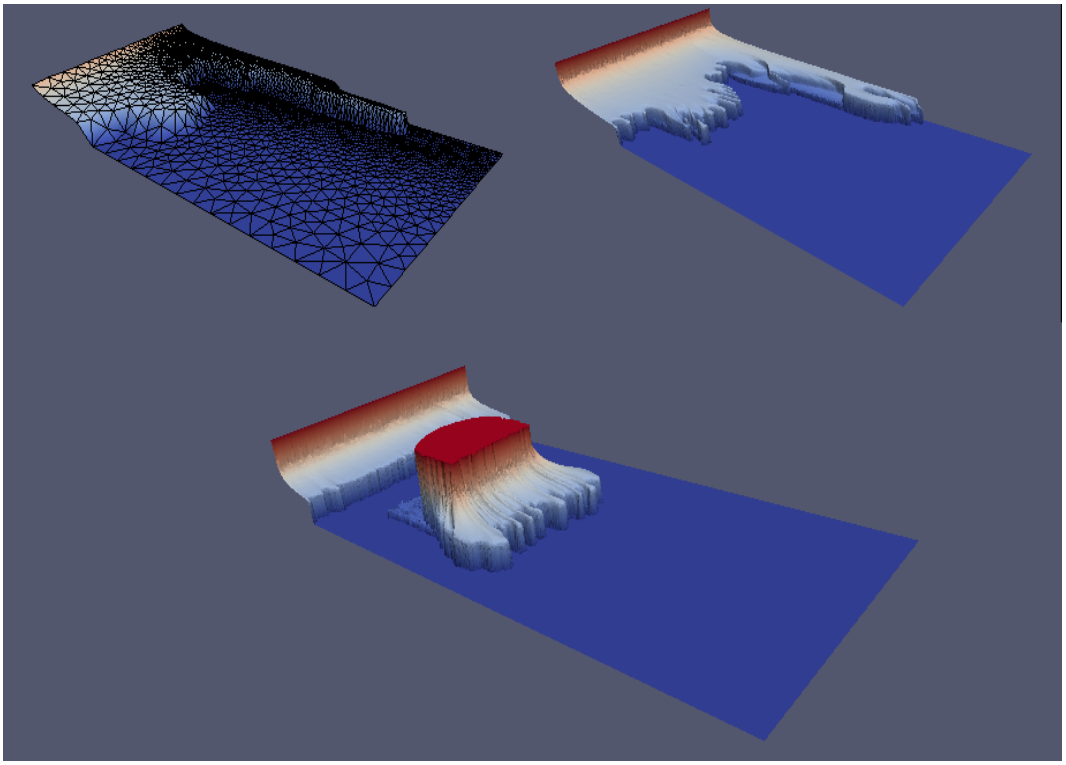

Figure 5: Snapshots of the simulations with fixed (top left) and adaptive mesh grids. Simulation performed with initial saturated media in the square-region is shown in the bottom.

3.2 Case 2: Heterogeneous Saturated/Unsaturated Porous Media

In the simulation performed here, the square-region ($\mathbf{K}_3 = 5$) is initially saturated with the injected Fluid 1. Figures 4 and 5 (bottom) show the trapped phase displacement during the injection. The initial shape of Fluid 1's front near the inlet are very similar to the cases studied in the previous section. At the top, it can be seen the first layer's flow (region with $\mathbf{K}_1 = 2$) developing faster and the second layer slightly slower. This behaviour can also be noticed in Fig. 4, where the velocity sharply increases from the smaller to the larger permeability region. Figure 4(c) shows that the saturation front has an inverse-exponential shape near the inlet, and then residual saturation at the high-permeability square (as enforced by the Corey expression for the relative permeability). The behaviour along the top two layers' interface is initially inverse exponential followed by an abrupt decrease in saturation front due to fingering. Saturation then increases quickly at the top layer, which will show a high velocity region.

4 CONCLUSIONS

This article summarises the new overlapping control volume finite element method for multi-fluid flows. The new formulation is based upon a dual consistent pressure-

velocity representation in CV and FEM spaces and a novel family of element types – $\mathrm{P}_n\mathrm{DGP}_{n+1}$. The aim of this paper is to further apply the formulation (embedded in the *Fluidity* software framework) to multiphase flows in heterogeneous porous media. The OCV-DGFEM was specially designed to ensure that for uniform viscous frictional forces – $\underline{\underline{\sigma}}_k = \mu_k S_k \left(\mathcal{K}_{rk}\mathbf{K}\right)^{-1}$, the balance in 1D Darcy multiphase flow equations is strictly enforced. Saturations are collocated (piecewise constant) in control volume space whereas permeabilities is piecewise constant in FE space to ensure the correct representation of the surface. In addition, the velocity field (for each phase) is described as a functional of $\underline{\underline{\sigma}}$ and pressure. For a quadratic pressure variation there will be a piecewise linear velocity field, with discontinuities at element and control volume boundaries. The formulation was able to simulate multiphase flows in heterogeneous porous media with unsaturated/saturated fluid distribution.

5 ACKNOWLEDGEMENT

Mr Radunz would like to acknowledge the support from the Brazilian Research Council, CNPq, under the *Science without Borders* scholarship programme.

REFERENCES

[1] C.J. Cotter, D.A. Ham and C.C. Pain. A mixed discontinuous/continuous finite element pair for shallow-water ocean modelling. *Ocean Modelling*, Vol. **26**, 86-90, 2009

[2] C.J. Cotter, D.A. Ham, C.C, Pain and S. Reich. LBB stability of a mixed discontinuous/continuous Galerkin finite element pair. *Journal of Computational Physics*, Vol. **228**, 336-348, 2009.

[3] C.J. Cotter and D.A. Ham. Numerical Wave Propagation for Triangular P1DG-P2 Finite Element Pair, *Journal of Computational Physics*, Vol. **230**, 2806-2820, 2011.

[4] P.A. Forsyth, Y.S. Wu and K. Pruess. Robust Numerical Methods for Saturated-Unsaturated Flow with Dry Initial Conditions in Heterogeneous Media. *Advances in Water Resources*, Vol. **18**, 25-38, 1995.

[5] J.L.M.A. Gomes, B. Tollit, B. Milles and C.C. Pain. Multi-Physics Flow Modelling for Nuclear Applications. *In Fluidization Engineering – Principles and Practice*, 2012.

[6] J.L.M.A. Gomes, D. Pavlidis, J.R. Percival, P. Mostaghimi, P. Salinas, X. Zie, C.C. Pain, M.D. Jackson and A. Muggeridge. The Overlapping Control Volume Finite Element Method for Multiphase Porous Media Flow Modelling – Part I: Formulation. *Computer Methods in Applied Mechanics and Engineering*, Submitted, 2013.

[7] S.K. Gupta, C.T. Kincaid, P.R. Mayer, C.A. Newbill and C.R. Cole. A multidimensional finite element code for the analysis of coupled fluid, energy and solute transport. *Technical Report PNL-2939*, Battelle Pacific Northwest Laboratory, 1982.

[8] G. M. Homsy. Viscous fingering in porous media. *Ann. Rev. Fluid Mech.*, Vol **19**, 271-31.

[9] M.D. Jackson, J.L.M.A. Gomes, P. Mostaghimi, J.R. Percival, B.S. Tollit, D. Pavlidis, C.C. Pain, A.H. El-Sheikh, A.H. Muggeridge, M.J. Blunt. Reservoir Modelling for Flow Simulation Using Surfaces, Adaptive Unstructured Meshes, and Control-Volume-Finite-Element Methods. *2013 SPE Reservoir Simulation Symposium*, **SPE163633**, 2013.

[10] C.C. Pain, A.P. Umpleby, C.R.E. Oliveira and A.J.H. Goddard. Tetrahedral mesh optimisation and adaptivity for steady-state and transient finite element calculations. *Computer Methods in Applied Mechanics and Engineering*, Vol.**190**, 3771-3796, 2001.

[11] M.D. Piggott, C.C. Pain, G.J. Gorman, P.W. Power and A.J.H. Goddard. h, r, and hr adaptivity with applications in numerical ocean modelling. *Ocean Modelling*, Vol. **10**, 95-113, 2005.

[12] W.E.H. Sollie and O. Bokhove. Space-Time Discontinuous Galerkin Finite Element Method for Two-Fluid Problems. *Journal of Computational Physics*, Vol. **141**, 46-77, 2006.

[13] P. Solin and M. Kuraz. Solving the nonstationary Richards equation with adaptive hp-FEM. *Advances in Water Resources*, Vol **34**, 1062-1081, 2011.

[14] E. Tzimas. Enhanced Oil Recovery using Carbon Dioxide in the European Energy System (PDF). *European Commission Joint Research Center*.

[15] Risk Assessment Guidance for Superfund, Human Health Evaluation Manual, *Report of the US Environmental Protection Agency, Office of Emergency and Remedial Response*, 1989.